

**Original citation:**

Zhao, B. (2012). Hard-input-hard-output capacity analysis of UWB BPSK systems with timing errors. IEEE Transactions on Vehicular Technology, 61(4), pp. 1741-1751.

**Permanent WRAP url:**

<http://wrap.warwick.ac.uk/49533>

**Copyright and reuse:**

The Warwick Research Archive Portal (WRAP) makes the work of researchers of the University of Warwick available open access under the following conditions. Copyright © and all moral rights to the version of the paper presented here belong to the individual author(s) and/or other copyright owners. To the extent reasonable and practicable the material made available in WRAP has been checked for eligibility before being made available.

Copies of full items can be used for personal research or study, educational, or not-for-profit purposes without prior permission or charge. Provided that the authors, title and full bibliographic details are credited, a hyperlink and/or URL is given for the original metadata page and the content is not changed in any way.

**Publisher's statement:**

“© 2012 IEEE. Personal use of this material is permitted. Permission from IEEE must be obtained for all other uses, in any current or future media, including reprinting/republishing this material for advertising or promotional purposes, creating new collective works, for resale or redistribution to servers or lists, or reuse of any copyrighted component of this work in other works.”

Zhao, B. (2012). Hard-input-hard-output capacity analysis of UWB BPSK systems with timing errors. IEEE Transactions on Vehicular Technology, 61(4), pp. 1741-1751.  
<http://dx.doi.org/10.1109/TVT.2012.2188418>

**A note on versions:**

The version presented here may differ from the published version or, version of record, if you wish to cite this item you are advised to consult the publisher's version. Please see the 'permanent WRAP url' above for details on accessing the published version and note that access may require a subscription.

For more information, please contact the WRAP Team at: [wrap@warwick.ac.uk](mailto:wrap@warwick.ac.uk)



# Hard-Input-Hard-Output Capacity Analysis of UWB BPSK Systems With Timing Errors

Bo Zhao, Yunfei Chen, *Senior Member, IEEE*, Roger J. Green, *Senior Member, IEEE*

Corresponding Address:

Yunfei Chen

School of Engineering

University of Warwick, Coventry, U.K. CV4 7AL

Tel: +44 (0)24 765 23105, e-mail: Yunfei.Chen@warwick.ac.uk

## Abstract

The hard-input-hard-output capacity of a binary phase shift keying ultra-wide bandwidth system is analyzed for both additive white Gaussian noise and multipath fading channels with timing errors. Unlike previous works that calculate the capacity with perfect synchronization and/or with multiple access interference only, our analysis consider timing errors with different distributions as well as the inter-path, inter-chip and inter-symbol interferences, as in practical systems. The sensitivity of the channel capacity to the timing error is examined. The effects of pulse shape, multiple access technique, number of users and number of chips are studied. It is found that time-hopping is less sensitive to the pulse shape and the timing error with higher capacity than direct-sequence due to its low duty of cycle. Using these results, one can choose appropriate system parameters for different applications.

## Index Terms

Channel capacity, synchronization, timing error, ultra-wide bandwidth.

Bo Zhao, Yunfei Chen and Roger J. Green are with the School of Engineering, University of Warwick, Coventry, U.K. CV4 7AL (e-mail: Bo.Zhao, Yunfei.Chen, Roger.Green@warwick.ac.uk). This work was presented in part at the International Conference on Ultra-Wideband in Nanjing, China in 2010 and in part at the International Symposium on Wireless Communications Systems in York, UK in 2010.

## I. INTRODUCTION

In recent years, ultra-wide bandwidth (UWB) technology has attracted great research interest from both academia and industry [1] [2]. Due to its very low transmission power, UWB is able to minimize interferences to coexist with other wireless systems in the same band. Thus, it is a very promising solution to wireless personal area networks and wireless sensor networks. In [3] - [6], performances of UWB systems have been analyzed in terms of the bit error rate (BER) and the signal-to-interference-plus-noise-ratio (SINR). In addition to BER and SINR, channel capacity is also an important performance measure that determines the maximum achievable information rate in a UWB system. Many researchers have analyzed the channel capacity for different UWB systems to provide useful engineering insights.

Based on the results for optical channels in [7], the channel capacity of an M-ary pulse position modulation (PPM) UWB system was evaluated in [8] for additive white Gaussian noise (AWGN) channels with a single user. For the same system, authors in [9] showed that the channel capacity is highly affected by pulse shapes. By modeling the multiple access interference (MAI) as Gaussian, the analysis on the channel capacity was extended to AWGN channels with multiple users in [10] - [13]. In [14], the channel capacities of pulse amplitude modulation (PAM) and PPM were compared over AWGN channels, where the MAI was also modeled as Gaussian. A different approximation that approximates the characteristic function of the MAI was adopted to evaluate the channel capacity of a binary PPM system in [15] and [16]. In addition, expressions for the channel capacities of direct sequence code division multiple access (DS-CDMA) and time-hopping (TH) PPM UWB systems were derived and compared in [17]. All these works calculate the channel capacity for AWGN channels. For multipath fading channels, the channel capacity has been analyzed for different UWB systems in [18] - [21]. It was shown in [18] and [19] that the random path energy and correlation in multipath fading channels cause significant capacity loss compared with the channel capacity in AWGN channels. Also, the inter-frame interference and the MAI reduce the channel capacity further for M-ary PPM UWB Rake systems [20], [21].

However, none of the aforementioned works has taken all the necessary interferences into account. It was reported in [22] that, in addition to the MAI, the inter-symbol interference (ISI), the inter-path interference (IPI) and the inter-chip interference (ICI) (or inter-frame interference) have significant effects on the performances of UWB systems too. The ISI is caused by displacements of different symbols, the ICI is caused by displacements of different chips in one symbol, while the IPI is caused by displacements of different multipath components in one chip. Also, stringent timing requirement is always a crucial issue for UWB communications, owing to the narrow pulse and the low transmission power. However, none of the aforementioned works has taken the timing error into account. It was shown in [23] that timing errors cause significant performance degradation to the BER. The same degradation to the symbol error rate was observed in [24] when time jitter is present. The degradation to channel capacity was not considered in [24] but will be presented in our work. In [25], the authors showed that this degradation can be reduced by choosing optimal processing gains for TH UWB systems. Similar degradations may also be observed for capacity. In [26], the impact of desynchronization between the local template and the received signal on the channel capacity was analyzed for UWB PPM systems over an AWGN channel with a single user. There still lacks a complete analysis of the channel capacity for UWB systems in the presence of timing errors corrupted by different interferences.

In this paper, we evaluate the capacity of DS and TH binary phase shift keying (BPSK) UWB systems in the presence of timing errors for a multi-user environment. Similar to [8]-[20], hard-input and hard-output capacity is calculated in our work. For simplicity, we refer to it as capacity in the following. Both AWGN and multipath fading channels are studied. In addition to the MAI, as in [14] - [16], the IPI, ICI and ISI are also considered. As well, different distributions of the timing error are examined for different pulse shapes. Numerical results show that the timing error can cause significant performance degradation in terms of channel capacity and that the amount of the degradation depends on several factors, including the distribution of the timing error, the pulse shape, the number of users and the number of chips. Although the channel capacity may not be amenable to practical system setting, our analysis is still useful by

providing engineers with insights and guidelines on the system design, for example, the number of users adopted in certain conditions.

## II. DS UWB

In this section, we will evaluate the capacity of a multi-user DS BPSK UWB system over AWGN and multipath fading channels. The transmitted signal of the  $k$ -th user can be expressed as

$$s_{tr}^{(k)}(t) = \sum_{m=-\infty}^{\infty} \sum_{n=0}^{N_c-1} b_m^{(k)} \beta_n^{(k)} g(t - mT_b - nT_c) \quad (1)$$

where  $b_m^{(k)}$  is the  $m$ -th data symbol of the  $k$ -th user and  $b_m^{(k)} = -1$  or  $b_m^{(k)} = +1$  with equal probabilities,  $\beta_n^{(k)}$  is the spreading code of the  $n$ -th frame of the  $k$ -th user and  $\beta_n^{(k)} = -1$  or  $\beta_n^{(k)} = +1$  with equal probabilities,  $T_c$  is the chip interval,  $N_c$  is the number of chips in each symbol,  $T_b = N_c T_c$  is the symbol interval, and  $g(t)$  is the monocycle pulse with energy  $E_g$  and duration  $D_g$ . Denote  $R_g(\cdot)$  as the normalized autocorrelation function of  $g(t)$ , normalized with respect to  $E_g$ , and  $R_g(\Theta) \approx 0$  when  $\Theta \geq D_g$  or  $\Theta \leq -D_g$ . In order to show that the sensitivity of channel capacity to the timing error is affected by the pulse shape, rectangular pulse, the second-order derivative Gaussian pulse and the fourth-order derivative Gaussian pulse are used as examples in our analysis. Then, one has

$$R_g(\Theta) = \begin{cases} 1 - \frac{|\Theta|}{D_g}, & 0 \leq |\Theta| \leq D_g \\ 0, & otherwise \end{cases}$$

when the rectangular pulse is used,

$$R_g(\Theta) = \left[ 1 - 4\pi \left( \frac{\Theta}{\nu} \right)^2 + \frac{4\pi^2}{3} \left( \frac{\Theta}{\nu} \right)^4 \right] e^{-\pi \left( \frac{\Theta}{\nu} \right)^2}$$

when the second-order derivative Gaussian pulse is used, and

$$R_g(\Theta) = \left[ 1 - 8\pi \left( \frac{\Theta}{\nu} \right)^2 + 8\pi^2 \left( \frac{\Theta}{\nu} \right)^4 - \frac{896\pi^3}{420} \left( \frac{\Theta}{\nu} \right)^6 + \frac{64\pi^4}{420} \left( \frac{\Theta}{\nu} \right)^8 \right] e^{-\pi \left( \frac{\Theta}{\nu} \right)^2}$$

when the fourth-order derivative Gaussian pulse is used, where  $\nu$  is a time scale factor. Assume that  $T_c \approx D_g$ .

### A. AWGN channel

Consider an AWGN channel first. Without loss of generality, the first user is treated as the desired user. Its superscript will be dropped for convenience in the following. Then, the received signal of the desired user is given by

$$r(t) = A \sum_{m=-\infty}^{\infty} \sum_{n=0}^{N_c-1} b_m \beta_n g(t - mT_b - nT_c - \tau) + \sum_{k=2}^{N_u} r^{(k)}(t) + n(t) \quad (2)$$

where  $r^{(k)}(t) = A^{(k)} s_{tr}^{(k)}(t - \tau^{(k)})$  is the interfering signal from the  $k$ -th user,  $n(t)$  is the AWGN with mean zero and standard deviation  $\sigma$ ,  $\tau$  and  $\tau^{(k)}$  are the transmission delays of the desired user and the  $k$ -th user, respectively,  $A$  and  $A^{(k)}$  are channel gains of the desired user and the  $k$ -th user, respectively. It is assumed that the interfering users have the same signal energy as the desired user through power control [27] and that  $\tau^{(k)}$  is uniformly distributed over  $[0, T_b)$ . When symbol-by-symbol detection is conducted, the memory in the channel does not need to be considered in the detection.

The receiver template for the detection of the  $\tilde{m}$ -th symbol of the desired user is given by

$$v(t) = \sum_{n'=0}^{N_c-1} \beta_{n'} g(t - n'T_c - \tilde{m}T_b - \hat{\tau}), \quad (3)$$

where  $\hat{\tau}$  is the timing estimate for the desired user. The output of the correlator can be derived as

$$R = \int_{\tilde{m}T_b + \hat{\tau}}^{(\tilde{m}+1)T_b + \hat{\tau}} r(t)v(t)dt = b_{\tilde{m}}S + I + \sum_{k=2}^{N_u} MAI_u^{(k)} + N \quad (4)$$

where  $S$  is the desired signal component,  $I = ISI + ICI$  includes the ICI and the ISI caused by the timing error  $\epsilon = \tau - \hat{\tau}$ ,  $MAI_u^{(k)}$  is the MAI from the  $k$ -th user and  $N$  is the noise component with

$$S = AN_c E_g R_g(\epsilon), \quad (5)$$

$$ISI = E_g b_{\tilde{m}-1} A \beta_{N_c-1} \beta_0 R_g(T_c - \epsilon), ICI = E_g b_{\tilde{m}} A R_g(T_c - \epsilon) \sum_{n=0}^{N_c-2} \beta_n \beta_{n+1}, \quad (6)$$

$$MAI_u^{(k)} = E_g \sum_{m=-\infty}^{\infty} \sum_{n=0}^{N_c-1} \sum_{n'=0}^{N_c-1} b_m^{(k)} A^{(k)} \beta_n^{(k)} \beta_{n'} R_g((m - \tilde{m})T_b + (n - n')T_c + \tau^{(k)} - \hat{\tau}). \quad (7)$$

It can also be shown that the variance of  $N$  is  $Z = \text{Var}\{N\} = \sigma^2 N_c E_g$ . Note that previous works on capacity analysis ignored  $I$ . Note also that the desired signal component will disappear when  $\epsilon \geq D_g$  or  $\epsilon \leq -D_g$ , as  $R_g(\epsilon) \approx 0$  in this case. The conditional means,  $E\{S^2|\epsilon\}$  and  $E\{I^2|\epsilon\}$ , and the value of  $E\{MAI_u^{(k)2}\}$  are calculated in Appendix A. For simplicity, the interference plus noise term is modeled as Gaussian. It will be shown later that, for both DS and TH systems, this approximation provides enough accuracy for our capacity analysis, and that it does not affect the analysis of the effect of the timing error on the channel capacity. Then, the conditional average BER, conditioned on  $\epsilon$ , is derived as

$$P_e(\epsilon) = Q \left( \sqrt{\frac{E\{S^2|\epsilon\}}{E\{I^2|\epsilon\} + E\{Z\} + (N_u - 1)E\{MAI_u^{(k)2}\}}} \right). \quad (8)$$

The capacity of a discrete memoryless channel using BPSK is given by [31]

$$C = \max_{P(x_j)} \sum_{j=0}^1 \sum_{i=0}^1 P(x_j) P(y_i|x_j) \log \frac{P(y_i|x_j)}{P(y_i)}, \quad (9)$$

where  $x_j$  represents the input symbols and  $y_i$  represents the output symbols. The maximum value of (9) is achieved when the system has equally likely input symbols in the binary modulation scheme [10], [19]. Therefore, the channel capacity for the desired user can be calculated as

$$C(\epsilon) = 1 + (1 - P_e(\epsilon)) \log_2(1 - P_e(\epsilon)) + P_e(\epsilon) \log_2 P_e(\epsilon). \quad (10)$$

Note from (9) that the channel capacity is determined by the transition probability, which depends on the BER. Since the BER is a function of the timing error in the analysis, the channel capacity is also parametrized by  $\epsilon$  when the timing error exists. By averaging (10) over  $\epsilon$ , the channel capacity of the desired user can be calculated as

$$\bar{C}_{AWGN} = \int_{-\infty}^{\infty} C(x) p_\epsilon(x) dx \quad (11)$$

where  $p_\epsilon(x)$  is the probability density function (PDF) of the timing error. Similar to [12], it is assumed that each user contributes a fraction of the traffic in the channel, so the total capacity is estimated by aggregating the channel capacity of each user. Then, in a multi-user environment, the total channel capacity can be estimated as [12]

$$\hat{C}_{AWGN} \approx N_u \cdot \bar{C}_{AWGN}. \quad (12)$$

One sees that  $\hat{C}_{AWGN}$  is proportional to the number of users  $N_u$ . But since  $\bar{C}_{AWGN}$  decreases with  $N_u$ , as can be seen from (8) to (11), the total capacity will be compromised by MAI. Using (8) and (10), the channel capacity of the desired user for the DS-BPSK UWB system in an AWGN channel can be calculated by (11), and the total channel capacity for the DS-BPSK UWB system can be calculated by (12).

### B. Multipath fading channel

Next, we will evaluate the capacity of the DS UWB system in a multipath fading channel with multiple users. The channel impulse response of the  $k$ -th user is  $h^{(k)}(t) = \sum_{l=0}^L \alpha_l^{(k)} \delta(t - \tau_l^{(k)})$  where  $\alpha_l^{(k)}$  and  $\tau_l^{(k)}$  are the path gain and the path delay of the  $l$ -th path for the  $k$ -th user, respectively, and  $\delta(\cdot)$  is the impulse function. Then, the received signal is

$$r(t) = \sum_{m=-\infty}^{\infty} \sum_{n=0}^{N_c-1} \sum_{l=0}^L b_m \beta_n \alpha_l g(t - mT_b - nT_c - \tau_l - \tau) + \sum_{k=2}^{N_u} r^{(k)}(t) + n(t) \quad (13)$$

where  $\alpha_l$  and  $\tau_l$  are the path gain and the path delay of the  $l$ -th path of the desired user, respectively,  $r^{(k)}(t)$  is the interfering signal from the  $k$ -th user with  $r^{(k)}(t) = s_{tr}^{(k)}(t - \tau^{(k)}) * h^{(k)}(t)$ ,  $n(t)$ ,  $\tau$  and  $\tau^{(k)}$  are defined as before. We assume perfect average power control as in [28] not instantaneous power control as in [29]. The receiver template for the  $\tilde{m}$ -th symbol of the desired user is given by

$$v(t) = \sum_{n'=0}^{N_c-1} \sum_{l=0}^L \beta_{n'} \tilde{\alpha}_l g(t - n'T_c - \tilde{m}T_b - \tilde{\tau}_l - \hat{\tau}), \quad (14)$$

where  $\tilde{\alpha}_l$  and  $\tilde{\tau}_l$  are estimates of the path gain and the path delay of the  $l$ -th path for the desired user, respectively. The correlator output is

$$R = b_{\tilde{m}}(S_D + IPI_D + ICI_D) + ISI_D + \sum_{k=2}^{N_u} MAI_{uD}^{(k)} + N_D \quad (15)$$

where  $S_D$ ,  $IPI_D$ ,  $ICI_D$ ,  $ISI_D$  and  $MAI_{uD}$  are the signal component, the inter-path interference, the inter-chip interference, the inter-symbol interference and the multiple access interference, respectively, given by

$$S_D = E_g N_c \sum_{l=0}^L \alpha_l \tilde{\alpha}_l R_g(\tau_l - \tilde{\tau}_l + \epsilon) \quad (16)$$



$$IPI_D = N_c E_g \sum_{l=0}^L \sum_{l'=0}^L \alpha_l \tilde{\alpha}_{l'} R_g(\tau_l - \tilde{\tau}_{l'} + \epsilon), \quad l \neq l' \quad (17)$$

$$ICI_D = E_g \sum_{l=0}^L \sum_{l'=0}^L \sum_{n=0}^{N_c-1} \sum_{n'=0}^{N_c-1} \alpha_l \tilde{\alpha}_{l'} \beta_n \beta_{n'} R_g(\tau_l - \tilde{\tau}_{l'} + (n - n')T_c + \epsilon), n \neq n' \quad (18)$$

$$ISI_D = E_g \sum_{m=-\infty}^{\infty} \sum_{l=0}^L \sum_{l'=0}^L \sum_{n=0}^{N_c-1} \sum_{n'=0}^{N_c-1} b_m \alpha_l \tilde{\alpha}_{l'} \beta_n \beta_{n'} R_g(\tau_l - \tilde{\tau}_{l'} + (n - n')T_c + (m - \tilde{m})T_b + \epsilon), m \neq \tilde{m} \quad (19)$$

$$MAI_{uD}^{(k)} = E_g \sum_{m=-\infty}^{\infty} \sum_{l=0}^L \sum_{l'=0}^L \sum_{n=0}^{N_c-1} \sum_{n'=0}^{N_c-1} b_m^{(k)} \alpha_l^{(k)} \tilde{\alpha}_{l'} \beta_n^{(k)} \beta_{n'} \cdot R_g(\tau_l^{(k)} - \tilde{\tau}_{l'} + (n - n')T_c + (m - \tilde{m})T_b + \tau^{(k)} - \hat{\tau}) \quad (20)$$

and  $N_D$  is the noise component with mean zero and variance

$$Z_D = \sigma^2 E_g \sum_{l=0}^L \sum_{l'=0}^L \sum_{n=0}^{N_c-1} \sum_{n'=0}^{N_c-1} \tilde{\alpha}_l \tilde{\alpha}_{l'} \beta_n \beta_{n'} R_g(\tilde{\tau}_l - \tilde{\tau}_{l'} + (n - n')T_c). \quad (21)$$

Note that the bit value of  $b_{\tilde{m}}$  appears in (15) as a common factor and therefore, it does not appear in (16) - (18) again. Similar to the analysis for the AWGN channel, the interference plus noise term is assumed Gaussian as in [20] and [23]. Thus, the conditional BER can be calculated as

$$\hat{P}_e(\epsilon) \approx Q \left( \sqrt{\frac{\int_{-\infty}^{\infty} S^2(\vec{x}|\epsilon) p_{\vec{d}}(\vec{x}) d\vec{x}}{\int_{-\infty}^{\infty} I(\vec{x}|\epsilon) p_{\vec{d}}(\vec{x}) d\vec{x} + (N_u - 1) \int_{-\infty}^{\infty} \int_0^{T_b} MAI_{uD}^{(k)2}(\vec{x}, y) p_{\vec{D}}(\vec{x}) p(y) dy d\vec{x}}} \right)}, \quad (22)$$

where  $I(\vec{x}|\epsilon) = IPI_D^2(\vec{x}|\epsilon) + ICI_D^2(\vec{x}|\epsilon) + ISI_D^2(\vec{x}|\epsilon) + Z_D(\vec{x}|\epsilon)$ ,  $\vec{d}$  and  $\vec{D}$  are vectors of  $\{\alpha_0, \tau_0, \tilde{\alpha}_0, \tilde{\tau}_0; \alpha_1, \tau_1, \tilde{\alpha}_1, \tilde{\tau}_1; \dots; \alpha_L, \tau_L, \tilde{\alpha}_L, \tilde{\tau}_L; b_m, \beta_n\}$  and  $\{\alpha_0^{(k)}, \tau_0^{(k)}, \tilde{\alpha}_0, \tilde{\tau}_0; \alpha_1^{(k)}, \tau_1^{(k)}, \tilde{\alpha}_1, \tilde{\tau}_1; \dots; \alpha_L^{(k)}, \tau_L^{(k)}, \tilde{\alpha}_L, \tilde{\tau}_L; b_m^k, \beta_n^{(k)}, \beta_n\}$ , respectively, and  $p(y) = \frac{1}{T_b}$  is the PDF of  $\epsilon^{(k)} = \tau^{(k)} - \hat{\tau}$ . Note that the integration over  $y$  in (22) is for  $\epsilon^{(k)}$ , the timing difference between the arrival time of the  $k$ -th interfering user and the timing estimate of the desired user. It is not for the timing error of the desired user  $\epsilon$ . From (22), previous works ignoring  $I(\vec{x}|\epsilon)$  are likely to overestimate the capacity. Since there are many random variables in (22), the conditional BER has to be calculated by simulation. One can calculate the Gaussian-Q function before the averaging but

it can be shown that this does not provide better accuracy. Using (22), the conditional channel capacity is

$$\hat{C}(\epsilon) = 1 + \hat{P}_e(\epsilon) \log_2(\hat{P}_e(\epsilon)) + (1 - \hat{P}_e(\epsilon)) \log_2(1 - \hat{P}_e(\epsilon)). \quad (23)$$

By averaging  $\hat{C}(\epsilon)$  over  $\epsilon$ , the channel capacity of the desired user in multipath fading channels is calculated as

$$\bar{C}_{fading} = \int_{-\infty}^{\infty} \hat{C}(x) p_\epsilon(x) dx. \quad (24)$$

The total channel capacity can be calculated as

$$\hat{C}_{fading} \approx N_u \cdot \bar{C}_{fading}. \quad (25)$$

Using (22) and (23), the channel capacity of the desired user for the DS-BPSK UWB system in a multipath fading channel can be calculated by using (24), and the total channel capacity for the DS-BPSK UWB system can be calculated by using (25).

### III. TH UWB

In this section, we will examine the capacity of a multi-user TH UWB system. In the TH UWB system, the transmitted signal of the  $k$ -th user is given by

$$s^{(k)}(t) = \sum_{m=-\infty}^{\infty} \sum_{n=0}^{N_s-1} b_m^{(k)} g(t - mT_b - nT_f - c_n^{(k)}T_c) \quad (26)$$

where  $T_f = N_h T_c$  is the frame duration,  $T_b = N_s T_f$  is the symbol interval,  $N_s$  is the number of frames in one symbol,  $N_h$  is the number of chips in each frame,  $c_n^{(k)} \in [0, N_h - 1]$  is the pseudo-random TH code of the  $k$ -th user, and all the other symbols are defined as before.

#### A. AWGN channel

In an AWGN channel, the received signal of the desired user is

$$r(t) = A \sum_{m=-\infty}^{\infty} \sum_{n=0}^{N_s-1} b_m g(t - mT_b - nT_f - c_n T_c - \tau) + \sum_{k=2}^{N_u} r^{(k)}(t) + n(t), \quad (27)$$

where  $r^{(k)}(t) = A^{(k)}s^{(k)}(t - \tau^{(k)})$  is the MAI from the  $k$ -th user. Then, the output of the correlator can be derived as

$$R = b_{\tilde{m}}S + I + \sum_{k=2}^{N_u} MAI_u^{(k)} + N. \quad (28)$$

It is easy to show that the expressions for  $S$  and  $N$  are the same as those in the DS-BPSK system. Also, the term of  $I$  can be ignored for large values of  $N_h$  and  $N_s$  in TH UWB, due to the low duty of cycle, as will be shown later. Thus, although the analysis is not exact by ignoring  $I$ , it is still very accurate. The MAI from the  $k$ -th user is

$$MAI_u^{(k)} = E_g \sum_{m=-\infty}^{\infty} \sum_{n=0}^{N_s-1} \sum_{n'=0}^{N_s-1} A^{(k)}b_m^{(k)} R_g((m - \tilde{m})T_b + (n - n')T_f + (c_n^{(k)} - c_{n'})T_c + \tau^{(k)} - \hat{\tau}) \quad (29)$$

where  $\tau^{(k)}$  is defined as before. The second-order moment of  $MAI_u^{(k)}$  can be shown as

$$E\{MAI_u^{(k)2}\} = E_g^2 A^{(k)2} \sum_{m=-\infty}^{\infty} \sum_{n_1, n_2=0}^{N_s-1} \sum_{n'_1, n'_2=0}^{N_s-1} E\{R_g(T_{m\tilde{m}} + T_{nn_1} + T_{cn_1} + \tau^{(k)} - \hat{\tau})R_g(T_{m\tilde{m}} + T_{nn_2} + T_{cn_2} + \tau^{(k)} - \hat{\tau})\}. \quad (30)$$

Using results in Appendix A, the BER is

$$P_e(\epsilon) = Q\left(\sqrt{\frac{A^2 E_g^2 N_s^2 R_g^2(\epsilon)}{\sigma^2 N_s E_g + (N_u - 1)E\{MAI_u^{(k)2}\}}}\right). \quad (31)$$

From (31), the BER decreases and therefore the channel capacity increases with  $A$ ,  $E_g$  and  $N_s$ . Then, using (31) in (10), the channel capacity of the desired user in AWGN channels for the TH-BPSK UWB system can be calculated by using (11), and the total channel capacity for the TH-BPSK UWB system can be calculated by using (12). Next, we discuss multipath fading channels.

### B. Multipath fading channel

In a multipath fading channel, one has the received signal as

$$r(t) = \sum_{m=-\infty}^{\infty} \sum_{n=0}^{N_s-1} \sum_{l=0}^L b_m \alpha_l g(t - mT_b - nT_f - c_n T_c - \tau_l - \tau) + \sum_{k=2}^{N_u} r^{(k)}(t) + n(t) \quad (32)$$

and the output of the correlator can be derived as

$$R = b_{\tilde{m}}(S_T + IPI_T + ICI_T) + ISI_T + \sum_{k=2}^{N_u} MAI_{uT}^{(k)} + N_T \quad (33)$$

where  $S_T$ ,  $IPI_T$ ,  $ICI_T$ ,  $ISI_T$  and  $MAI_{uT}$  represent the signal component, the inter-path interference, the inter-chip interference, the inter-symbol interference and the multiple access interference, respectively. It is easy to show that the expressions of  $S_T$  and  $IPI_T$  are the same as  $S_D$  in (16) and  $IPI_D$  in (17), respectively. On the other hand, the expressions for  $ICI_T$ ,  $ISI_T$ ,  $Var\{N_T\}$  and  $MAI_{uT}^{(k)}$  are given by

$$ICI_T = E_g \sum_{n,n'=0}^{N_s-1} \sum_{l,l'=0}^L \alpha_l \tilde{\alpha}_{l'} R_g((n - n')T_f + (c_n - c_{n'})T_c + \tau_l - \tilde{\tau}_{l'} + \epsilon), \quad n \neq n', \quad (34)$$

$$ISI_T = E_g \sum_{m=-\infty}^{\infty} \sum_{n,n'=0}^{N_s-1} \sum_{l,l'=0}^L b_m \alpha_l \tilde{\alpha}_{l'} R_g((m - \tilde{m})T_b + (n - n')T_f + (c_n - c_{n'})T_c + \tau_l - \tilde{\tau}_{l'} + \epsilon), \quad m \neq \tilde{m}, \quad (35)$$

$$Var\{N_T\} = Z_T = \sigma^2 E_g \sum_{n,n'=0}^{N_s-1} \sum_{l,l'=0}^L \tilde{\alpha}_l \tilde{\alpha}_{l'} R_g((n - n')T_f + (c_n - c_{n'})T_c + \tilde{\tau}_l - \tilde{\tau}_{l'}) \quad (36)$$

and

$$MAI_{uT}^{(k)} = E_g \sum_{m=-\infty}^{\infty} \sum_{l=0}^L \sum_{l'=0}^L \sum_{n=0}^{N_s-1} \sum_{n'=0}^{N_s-1} b_m^{(k)} \alpha_l^{(k)} \tilde{\alpha}_{l'} \cdot R_g((m - \tilde{m})T_b + (n - n')T_f + (c_n^{(k)} - c_{n'})T_c + \tau_l^{(k)} - \tilde{\tau}_{l'} + \tau^{(k)} - \hat{\tau}) \quad (37)$$

respectively. Then, the channel capacity of the desired user for the TH-BPSK UWB system in multipath fading channels can be calculated by using (16), (17) and (34) - (37) in (22) together with (24), and the total channel capacity for the TH-BPSK UWB system can also be calculated by using (25).

#### IV. NUMERICAL RESULTS AND DISCUSSION

In this section, numerical results are presented to show the effect of the timing error on the channel capacity of the BPSK UWB systems. In the calculation, assume that  $A = 1$ ,  $D_g = 1$  ns

and the timing error  $\epsilon$  is distributed over  $[-T_c, T_c]$  as the desired signal component will disappear when  $\epsilon \geq T_c$  or  $\epsilon \leq -T_c$  and the timing error will be too large to be meaningful for signal detection or performance analysis. The IEEE CM1 and CM2 UWB channel models [32] are used for multipath fading. Numbers of 20 and 34 multipath components are used for CM1 and CM2 channel models, respectively, which are enough to achieve almost 85% of the channel gain [32]. Also, consider the case when channel estimation is implemented to estimate the path gains and path delays of the multipath components in the fading channels and estimation errors occur that are Gaussian distributed with means equal to the true values and standard deviations equal to 0.2 for gains and 0.05 for delays, as reported in [33]. This setting aims to make the simulation results closer to engineering practice. All the values of SNR in the paper refers to the input SNR except in Fig. 8 that uses the output SNR.

Fig. 1 compares the channel capacity for different pulse shapes with a single user over AWGN channels. Assume that the timing error is uniformly distributed in the comparison and that  $N_c$  is fixed at 6. The rectangular pulse serves as a benchmark. The fourth-order derivative Gaussian pulse meets the Federal Communications Commission (FCC) spectrum mask [34], while the second-order derivative Gaussian pulse has been commonly used in UWB analysis. One sees that the channel capacity increases when the SNR increases, and that it approaches an upper limit when the SNR is large. Comparing the channel capacity for different pulse shapes, one sees that the rectangular pulse has the largest capacity, while the second-order derivative Gaussian pulse and the fourth-order derivative Gaussian pulse have smaller capacities. Mathematically, this is because the value of the autocorrelation of the rectangular pulse is larger than those of the autocorrelations of the other two pulses for the same  $\Theta$ . Intuitively, this is because the pulse energy is more confined for the rectangular pulse and thus, it incurs less interferences. Therefore, timing error causes less capacity loss for the rectangular pulse than for the second-order derivative Gaussian pulse and the fourth-order derivative Gaussian pulse. One also sees that there is a large performance difference near the upper limit. This is due to the error floor caused by interference, which dominates for large values of  $SNR$ . In these regions, it is more useful

to observe whether the error floor is reduced than to observe the actual value of performance difference. As well, the TH-BPSK system is less sensitive to the pulse shape than the DS-BPSK due to its low duty of cycle leading to less interferences in this case. Since the second-order derivative Gaussian pulse is commonly used in literature, it will be adopted in the following to examine the effects of other system parameters.

Fig. 2 shows the effect of the timing error on the channel capacity of the DS-BPSK system in an AWGN channel for different distributions of the timing error. We set  $N_c = 6$ . In addition to the uniform distribution and the Gaussian distribution, the typical Tikhonov distribution for timing error is also used [35], [36]. One sees that the timing error causes significant performance degradation to the channel capacity. The channel capacity is the lowest for uniformly distributed timing error, while the highest for Gaussian distributed timing error. This is due to the fact that the kurtosis of the Gaussian distribution is the largest while the kurtosis of the uniform distribution is the smallest, and higher kurtosis gives timing error closer to zero which results in a stronger signal component. Most well-designed synchronizers follow an asymptotic Gaussian distribution when the sample size is large [37]. Note that, in practice, the timing error distribution is implementation dependent and thus we cannot control the distribution.

Fig. 3 shows the effect of the number of users on the channel capacity per user for the DS-BPSK system in an AWGN channel. Both analytical and simulation results are presented. We set  $N_c = 10$  and  $SNR = 6$  dB, and the number of users starts from 10. One sees that the analytical results are very close to the simulation results in all the cases. Comparing channel capacity for different timing error distributions, one sees that there is a capacity loss of 76% when the number of users increases from 10 to 100 and timing error is Gaussian distributed, while there are capacity losses of 77% and 80%, respectively, for Tikhonov distributed timing error and uniformly distributed timing error. This is because the signal component in the output of the correlator is stronger for the Gaussian distribution than for the Tikhonov distribution and the uniform distribution. Fig. 4 shows the total channel capacity of the same system for all users in an AWGN channel. It can be seen that the Gaussian distribution has the highest total

capacity while the uniform distribution has the lowest total capacity. Moreover, the total capacity increases with a decrease of variance in the Gaussian distribution.

Fig. 5 shows the effect of the interferences and the timing error on the channel capacity of the DS-BPSK system in the multipath fading channel with a single user. The CM1 channel model is used. The SNR increases from  $-10$  dB to  $42$  dB. We set  $N_c = 6$ . Simulation results for uniform distributed timing error are also presented, and it is seen that our semi-analytical results are close to the simulation results. One also sees that both the timing error and the interferences cause significant degradation in the channel capacity. Analogous to [18], [19] and [28], the channel capacity in the multipath fading channel is lower than that in the AWGN channel, under the same conditions. Comparing the effect of the timing error on the channel capacities for the multipath fading channel and the AWGN channel, one sees that the detrimental effect of the timing error is more severe in the multipath fading channel than in the AWGN channel. Therefore, it is more important to achieve accurate synchronization for the DS-BPSK system in the multipath fading channel than in the AWGN channel. For the same system, Fig. 6 shows the channel capacity in the CM2 channel model. Comparing the channel capacity in CM2 with that in CM1, one sees that the channel capacity in the CM1 channel model is slightly higher than that in the CM2 channel model, under the same conditions. In addition, it is seen that the interferences have more significant effects on the channel capacity in the CM2 channel model than that in the CM1 channel model. For example, at  $0.8$  bits/symbol, CM1 has a loss of  $9$  dB due to interferences while CM2 has a loss of  $15$  dB. This is expected. The CM2 channel model does not have a line-of-sight and the interferences caused by multipath components are stronger in CM2 than those in CM1.

Fig. 7 shows the total channel capacity in the CM1 channel model. We set  $SNR = 6$  dB and  $N_c = 10$ . The number of users increases from  $10$  to  $490$ . One sees that the total channel capacity in the multipath fading channel has similar behaviors to those in the AWGN channel. Also, the total channel capacity in the multipath fading channel is lower than that in the AWGN channel, which agrees with previous observations. One also sees that the TH-BPSK system is

less sensitive to the timing error or its capacity is larger than the DS-BPSK due to the low duty of cycle with less interferences in this case.

Fig. 8 examines the effect of  $I$  on the output SINR of the TH-BPSK system in a single user AWGN channel for different values of  $N_s$ . The value of  $N_h$  increases from 3 to 10. The value of input SNR represents the transmitted signal strength and is set at 18 dB so that the noise is not dominant and the impact of  $I$  on the output SINR can be clearly observed. It is assumed that the timing error is uniformly distributed as this is the worst case. The output SNR is around 9.1 dB, which represents the received signal strength averaged over the timing error and it is different from the input SNR set at 18 dB as the transmitted signal strength. One sees that the difference between the output SNR and the output SINR for the same value of  $N_s$  decreases when  $N_h$  increases, in all the cases considered. This implies that the value of  $I$  is negligible when  $N_h$  is large, because the only difference between SNR and SINR is the value of  $I$ . Furthermore, comparing the difference between the output SNR and the output SINR when  $N_s = 6$  with that when  $N_s = 10$ , one sees that a larger value of  $N_s$  results in a smaller difference. This indicates that the value of  $I$  decreases when  $N_s$  increases. Consequently,  $I$  can be ignored in the TH-BPSK system when the values of  $N_h$  and  $N_s$  are large, mainly due to the low duty of cycle. The ISI depends on the frame duration but  $T_f = N_h T_c$  and  $T_c$  is fixed in Fig. 8, so the effect of  $T_f$  is the same as  $N_h$ .

Fig. 9 shows the relationship between the number of users and the channel capacity per user for the TH-BPSK system over AWGN channels. We set  $N_s = 6$  and the SNR is 6 dB. Both analytical and simulation results are presented. One sees that the analytical results track the trends of the simulation results well and that the approximation error is small for small values of the number of users. However, in general, the approximation error is large due to the lower duty of cycle [38]. Also, one sees that a larger value of  $N_h$  results in a larger channel capacity. Therefore, the capacity loss caused by the MAI or the timing error can be reduced by increasing  $N_h$ . For the same system, Fig. 10 shows the relationship between the number of users and the total channel capacity for all users in an AWGN channel. The more impulsive the timing error



distribution is, the larger the increment of the total channel capacity will be. One sees that a larger  $N_h$  results in a higher increment.

Fig. 11 compares the effect of the interferences and the timing error with different distributions on the channel capacity of the TH-BPSK system in the CM1 channel model. We set  $N_s = 6$  and  $N_h = 6$ . The SNR increases from  $-10$  dB to  $42$  dB. Simulation results for uniformly distributed timing error are also presented. It is observed that our semi-analytical results are close to the simulation results when the SNR is small while there are approximation errors when the SNR is large. Similar to the channel capacity of the DS-BPSK system, one sees that both the interferences and the timing error cause significant effects on the channel capacity. As well, when the timing error and interferences are present, the channel capacity of the TH-BPSK system in the multipath fading channel approaches an upper limit when the SNR is large. The processing gain of DS-BPSK in Fig. 5 equals  $N_c = 6$ , which is the same as the processing gain  $N_s = 6$  of TH-BPSK in Fig. 11. Compared with DS-BPSK in Fig. 5, one also sees that TH-BPSK has higher capacity for the same SNR value and the same timing error distribution. This is because time-hopping incurs less interferences than direct-sequence due to its very low duty of cycle such that capacity degradation from interferences is also reduced. For the same system, Fig. 12 shows the relationship between the number of users and the total channel capacity in the CM1 channel model. We set  $SNR = 6$  dB. Again, TH-BPSK has higher total capacity and can accommodate more users than DS-BPSK system.

The numerical results have illustrated the impact of the number of users on both the channel capacity and the total channel capacity. This can be used by engineers to design a multiple access strategy by setting an upper limit for the number of users with maximum total channel capacity while minimizing the impact of the MAI on the channel capacity for each user. The result in this paper can be easily extended to binary PPM UWB systems by changing the modulation format in the signal models. The analysis method is similar, but some conclusions might be different as PPM has a lower duty of cycle. The result in this paper assumes the Gaussian approximation to the MAI, IPI, ICI and ISI. It was reported in [38] that better PDFs of the MAI for TH-PPM

exist for small  $N_u$  and small  $N_s$  but Gaussian approximation is valid for large  $N_u$  and  $N_s$  in [39] and [40], in dense multipath even for single user with small  $N_s$  [40], [41], as well as for DS systems and TH systems with large numbers of interfering users [38]. It was also reported in [42] that a Laplacian approximation to the IPI, ICI and ISI gives better accuracy than the Gaussian approximation for large SNRs while they have similar accuracy when the SNR is less than 10 dB. When the MAI, IPI, ICI and ISI are modeled as non-Gaussian distributions, such as a Laplacian distribution, the accuracy of the capacity analysis may be improved by replacing the Gaussian Q function in (8), (22) and (31) with other corresponding functions, such as a mixture of Gaussian-Q functions [42]. Due to the similarity of the analysis, they are not presented here. Reference [5] performed a statistical analysis of the interference powers for DS-BPSK in multipath fading without timing error, while this paper uses a similar method for both DS-BPSK and TH-BPSK in AWGN and multipath fading with timing error. None of the results in this paper are the same as those in [5].

Note that the above analysis considers hard-output capacity based on (9) instead of soft-output capacity. First, the work is presented as a much more complete analysis than [8]- [20] that used hard-output capacity. Thus, it uses the same capacity definition to facilitate comparison if one wants. Second, by using (9), one has a direct relationship between capacity and error rate. Third, unlike the soft-output capacity that only considers the propagation channel, the hard-output capacity considers the whole system by including modulation and demodulation as part of the equivalent channel. It is well known that for systems with large operating bandwidths, such as UWB systems, the soft-output capacity may not be a proper metric, as they only consider the propagation channel [43], while hard-output capacity takes the whole system into account and therefore, is more useful in this case. It is very challenging to derive the soft-output capacity and the exact hard-output capacity by taking the timing error and all the interferences into account.

## APPENDIX A

CALCULATION OF  $E\{S^2|\epsilon\}$ ,  $E\{I^2|\epsilon\}$  AND  $E\{MAI_u^{(k)2}\}$ 

In this appendix, we calculate  $E\{S^2|\epsilon\}$ ,  $E\{I^2|\epsilon\}$  and  $E\{MAI_u^{(k)2}\}$ .

From (5),  $E\{S^2|\epsilon\} = A^2 E_g^2 N_s^2 R_g^2(\epsilon)$ . From (6), one has

$$E\{I^2|\epsilon\} = A^2 E_g^2 R_g^2(T_c - \epsilon) E\{1 + \{\sum_{n=0}^{N_c-2} \beta_n \beta_{n+1}\}^2\}. \quad (38)$$

Since  $E\{\{\sum_{n=0}^{N_c-2} \beta_n \beta_{n+1}\}^2\} = N_c - 1$ , one has

$$E\{I^2|\epsilon\} = N_c A^2 E_g^2 R_g^2(T_c - \epsilon). \quad (39)$$

Also, from (7), one can have

$$\begin{aligned} E\{MAI_u^{(k)2}\} &= E_g^2 A^{(k)2} E\left\{ \sum_{m_1=-\infty}^{\infty} \sum_{m_2=-\infty}^{\infty} \sum_{n_1=0}^{N_c-1} \sum_{n_2=0}^{N_c-1} \sum_{n'_1=0}^{N_c-1} \sum_{n'_2=0}^{N_c-1} b_{m_1}^{(k)} b_{m_2}^{(k)} \right. \\ &\quad \left. \beta_{n_1}^{(k)} \beta_{n_2}^{(k)} \beta_{n'_1} \beta_{n'_2} \cdot R_g((m_1 - \tilde{m})T_b + (n_1 - n'_1)T_c + \tau^{(k)} - \hat{\tau}) \right. \\ &\quad \left. \cdot R_g((m_2 - \tilde{m})T_b + (n_2 - n'_2)T_c + \tau^{(k)} - \hat{\tau}) \right\}. \end{aligned} \quad (40)$$

Since  $E\{b_{m_1}^{(k)} b_{m_2}^{(k)}\} = 0$  for  $m_1 \neq m_2$ ,  $E\{\beta_{n_1}^{(k)} \beta_{n_2}^{(k)}\} = 0$  for  $n_1 \neq n_2$  and  $E\{\beta_{n'_1} \beta_{n'_2}\} = 0$  for  $n'_1 \neq n'_2$ , it can be derived that

$$E\{MAI_u^{(k)2}\} = E_g^2 A^{(k)2} \sum_{m=-\infty}^{\infty} \sum_{n=0}^{N_c-1} \sum_{n'=0}^{N_c-1} E\{R_g^2(T_{m\tilde{m}} + T_{nn'} + \tau^{(k)} - \hat{\tau})\}, \quad (41)$$

where  $T_{m\tilde{m}} = (m - \tilde{m})T_b$  and  $T_{nn'} = (n - n')T_c$ . Define

$$\xi_{m\tilde{m}nn'} = T_{m\tilde{m}} + T_{nn'} + \tau^{(k)} - \hat{\tau}.$$

Since  $\epsilon^{(k)} = \tau^{(k)} - \hat{\tau}$  is uniformly distributed over a symbol interval,  $\xi_{m\tilde{m}nn'}$  is uniformly distributed over  $[T_{m\tilde{m}} + T_{nn'}, T_{m\tilde{m}} + T_{nn'} + T_b]$ . For convenience,  $\xi_{m\tilde{m}nn'}$  is simplified to  $\xi$ . When the second-order derivative Gaussian pulse is used,  $E\{R_g^2(\xi)\}$  can be derived as

$$\begin{aligned} E\{R_g^2(\xi)\} &= \frac{1}{E_g^2} E\left\{ \frac{9}{256} \exp(-8\pi\xi^2/D_g^2) - \frac{9\pi\xi^2}{8D_g^2} \exp(-8\pi\xi^2/D_g^2) \right. \\ &\quad \left. + \frac{12\pi^2\xi^4}{8D_g^4} \exp(-8\pi\xi^2/D_g^2) + \frac{9\pi^2\xi^4}{D_g^4} \exp(-8\pi\xi^2/D_g^2) \right. \\ &\quad \left. - \frac{24\pi^3\xi^6}{D_g^6} \exp(-8\pi\xi^2/D_g^2) + \frac{16\pi^4\xi^8}{D_g^8} \exp(-8\pi\xi^2/D_g^2) \right\}. \end{aligned} \quad (42)$$

After some simple but tedious mathematical manipulations, every term on the right side of (42) can be solved. Then,  $E\{MAI_u^{(k)2}\}$  can be calculated.

## REFERENCES

- [1] M. Win and R. Scholtz, "Impulse radio: how it works," *IEEE Commun. Lett.*, vol. 2, pp. 36-38, Feb. 1998.
- [2] S. Roy, J. R. Foerster, V. S. Somayazulu and D. G. Leeper, "Ultra-wideband radio design: The promise of high-speed, short-range wireless connectivity," Invited Paper, *Proc. IEEE*, vol. 92, no. 2, pp. 295-311, Feb. 2004.
- [3] L. Zhao, A. M. Haimovich, "Performance of ultra-wideband communications in the presence of interference," *IEEE J. Select. Areas Commun.*, vol. 20, no. 9, pp. 1684-1691, Dec. 2002.
- [4] Y. Chen and N. C. Beaulieu, "SNR estimation methods for UWB systems," *IEEE Trans. Wireless Commun.*, vol. 6, pp. 3836-3845, Oct. 2007.
- [5] B. Zhao, Y. Chen and R. J. Green, "Average SINR analysis of DS-BPSK UWB systems with IPI, ICI, ISI, MAI and its application," *IEEE Trans. Veh. Technol.*, vol. 58, no. 8, pp. 4690-4696, Oct. 2009.
- [6] T. Jia and D.I. Kim, "Analysis of channel-averaged SINR for indoor UWB rake and transmitted reference systems," *IEEE Trans. Commun.*, vol. 55, no. 10, pp. 2022-2032, Oct. 2007.
- [7] S. Dolinar, D. Divsalar, J. Hamkins and F. Pollara, "Capacity of PPM on Gaussian and Webb channels," *JPL TMO Progress Report*, vol. 42-142, pp. 1-31, Apr.-Jun. 2000.
- [8] L. Zhao, A. M. Haimovich, "Capacity of M-ary PPM ultra-wideband communications over AWGN channels," *Proceedings of VTC 2001 fall*, Oct. 7-11 2001, Atlantic City, New Jersey.
- [9] M. Abdel-Hafez, F. Alagöz, M. Hämäläinen and M. Latva-Aho, "On UWB capacity with respect to different pulse waveforms," *WOCN 2005. Second IFIP International Conference*, pp. 107-111, Mar. 2005.
- [10] J. Zhang, R. A. Kennedy and T. D. Abhayapala, "New results on the capacity of M-ary PPM ultra- wideband systems," *IEEE International Conf. on Communications (ICC)*, vol. 4, pp. 2867-2871, May 2003.
- [11] L. Zhao, A. M. Haimovich, "The capacity of an UWB multi-access communications system," *IEEE International Conf. on Communications (ICC)*, vol. 3, pp. 1964-1968, 28 Apr. - 2 May 2002.
- [12] L. Zhao, A. M. Haimovich, "Multi-user capacity of M-ary PPM ultra-wideband communications," *Proc. IEEE Conf. Ultra Wideband Systems, Technologies*, pp.175-179, May 20-23 2002, Baltimore, MD.
- [13] A. Adinoyi and H. Yanikomeroglu, "Practical capacity calculation for time-hopping ultra-wide band multiple-access communications," *IEEE Commun. Lett.*, vol.9, no.7, pp.601-603, Jul. 2005.
- [14] H. Zhang and T. A. Gulliver, "Performance and capacity of PAM and PPM UWB time-hopping multiple access communications with receiver diversity," *EURASIP J. Applied Signal Proc.*, vol. 2005, no. 3, pp. 306-315, Mar. 2005.
- [15] R. Pasand, S. Khaleshosseini, J. Nielsen and A. Sesay, "The capacity of asynchronous M-ary time hopping PPM UWB multiple access communication systems," *Proc. Vehicular Technology Conference,(VTC2004-Fall)*, vol. 7, pp. 4745-4749, Sept. 2004.

- [16] R. Pasand, S. Khaleshosseini and J. Nielsen, "Performance analysis of synchronous M-ary time-hopping PPM UWB multiple-access communication systems," *CCECE/CCGEI. 2005*, pp. 1212-1216, May 2005.
- [17] M. Abdel-Hafez and F. Alagöz, "Capacity of DS-CDMA versus TH-PPM for multi-user ultra-wideband systems," *IEEE International Symposium on Personal, Indoor and Mobile Radio Communication (PIMRC'06)*, pp. 1-5, Sept. 2006.
- [18] F. Ramirez-Mireles, "On the capacity of UWB over multipath channels," *IEEE Commun. Lett.*, vol. 9, no. 6, pp. 523-525, Jun. 2005.
- [19] T. Erseghe, "Capacity of UWB impulse radio with single-user reception in Gaussian noise and dense multipath," *IEEE Trans. Commun.*, vol. 53, no. 8, pp. 1257-1262, Aug. 2005.
- [20] N. Güney, H. Deliç, and F. Alagöz, "Achievable information rates of M-ary PPM impulse radio for UWB channels and Rake reception," *IEEE Trans. Commun.*, vol. 58, no. 5, pp. 1524-1535, May 2010.
- [21] F. Ramirez-Mireles, "Performance of UWB N-Orthogonal PPM in AWGN and multipath channels" *IEEE Trans. Veh. Technol.*, vol. 56, no. 3, pp. 1272-1285, May 2007.
- [22] Y. Chen and N.C. Beaulieu "Interference analysis of UWB systems for IEEE channel models using first- and second-order moments," *IEEE Trans. Commun.*, vol. 57, no. 3, pp. 622-625, Mar. 2009.
- [23] Z. Tian and G. B. Giannakis, "BER sensitivity to mistiming in Ultra-Wideband impulse radios - Part I: nonrandom channels," *IEEE Trans. on Signal Proc.*, vol. 53, no. 4, pp. 1550-1560, Apr. 2005.
- [24] N. V. Kokkalis, P. T. Mathiopoulos, G. K. Karagiannidis and C. S. Koukourlis, "Performance analysis of M-ary PPM TH-UWB systems in the presence of MUI and timing jitter," *IEEE J. Select. Areas Commun.*, vol. 24, no. 4, pp. 822-828, Apr. 2006.
- [25] S. Gezici, A. F. Molisch, H. V. Poor and H. Kobayashi "The tradeoff between processing gains of an impulse radio UWB system in the presence of timing jitter," *IEEE Trans. Commun.*, vol. 55, no. 8, pp. 1504-1511, Aug. 2007.
- [26] M. Kamoun, M. Courville, L. Mazet and P. Duhamel, "Impact of desynchronization on PPM UWB systems: a capacity based approach," *IEEE Information Theory Workshop 2004*, pp. 198-203, 24-29 Oct. 2004.
- [27] B. Hu and N. C. Beaulieu, "Exact bit error rate analysis of TH-PPM UWB systems in the presence of multiple access interference," *IEEE Commun. Lett.*, vol. 7, no. 12, pp. 572-574, Dec. 2003.
- [28] F. Ramirez-Mireles, "Quantifying the degradation of combined MUI and multipath effects in impulse-radio UWB," *IEEE Trans. on Wireless Commun.*, vol. 6, pp. 2831-2836, Aug. 2007.
- [29] R. Knopp, P.A. Humblet, "Information capacity and power control in single-cell multiuser communications," *Proc. IEEE ICC 1995*, vol. 1, pp. 331-335, Seattle, USA, 1995.
- [30] B. Hu and N. C. Beaulieu, "Accurate performance evaluation of time-hopping and direct-sequence UWB systems in multi-user interference," *IEEE Trans. Commun.*, vol. 53, no. 6, pp. 1053-1062, Jun. 2005.
- [31] J. G. Proakis, *Digital Communication*, 3rd ed. London, U.K.: McGraw-Hill, 1995.
- [32] "Channel modeling sub-committee report final," IEEE P802.15-02/368r5-SG3a, Dec. 2002.
- [33] V. Lottici, A. D'Andrea and U. Mengali, "Channel estimation for ultra-wideband communications," *IEEE J. Select. Areas Commun.*, vol. 20, pp. 1638-1654, Dec. 2002.

- [34] B. Hu and N. C. Beaulieu, "Pulse shapes for Ultrawideband communication systems," *IEEE Trans. Wireless Commun.*, vol. 4, no. 4, pp. 1789-1797, Jul. 2005.
- [35] M. Moeneclaey, "The influence of four types of symbol synchronizers on the error probability of a PAM receiver," *IEEE Trans. Commun.*, vol. 32, no. 11, pp. 1186-1190, Nov. 1984.
- [36] K. Bucket and M. Moeneclaey, "Effect of random carrier phase and timing errors on the detection of narrowband M-PSK and bandlimited DS/SS M-PSK signals," *IEEE Trans. Commun.*, vol. 43, no. 2/3/4, pp. 1260-1263, Feb.-Mar.-Apr. 1995.
- [37] U. Mengali and A. N. D'Andrea, *Synchronization Techniques for Digital Receivers*, New York, Plenum Press, 1997.
- [38] N. C. Beaulieu and D. J. Young, "Designing time-hopping ultra-wide bandwidth receivers for multi-user interference environments," Invited Paper, *Proc. IEEE*, vol. 97, no. 2, pp. 255-283, Feb. 2009.
- [39] Y. Dhibi and T. Kaiser, "On the impulsiveness of multiuser interferences in TH-PPM-UWB systems," *IEEE Trans. on Signal Proc.*, vol. 54, no. 7, pp. 2853-2857, Jul. 2006.
- [40] F. Ramirez-Mireles and A. Almada, "Testing the Gaussianity of UWB TH-PPM MUI with imperfect power control and multipath," *Proc. 5th International Conf. on Electrical Engineering, Computing Science and Automatic Control*, pp. 242-247, 12-14 Nov. 2008.
- [41] Q.T. Zhang and S.H. Song, "Parsimonious correlated nonstationary models for real baseband UWB data", *IEEE Trans. on Veh. Technol.*, vol. 54, pp. 447-455, Mar. 2005.
- [42] H. Shao and N.C. Beaulieu, "An analytical method for calculating the bit error rate performance of Rake reception in UWB multipath fading channels," *Proc. ICC 2008*, pp. 4855-4860, Beijing, China, May 2008.
- [43] T.S. Sakar, S. Burintramart, N. Yilmazer, H. Seunghyeon, Y. Zhang, A. De, M. Salazar-Palma, "A discussion about some of the principles/practices of wireless communication under a Maxwellian framework," *IEEE Trans. Antennas and Propagations*, vol. 54, pp. 3727 - 3745, Dec. 2006.

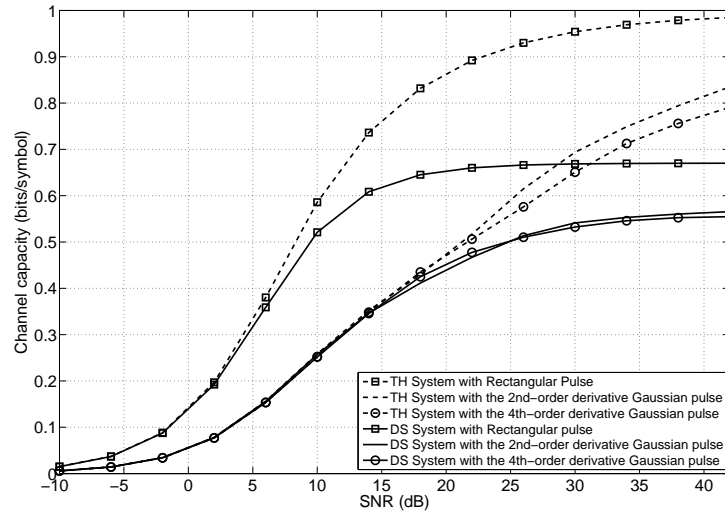


Fig. 1. Channel capacity v.s. SNR for different pulse shapes in DS-BPSK and TH-BPSK systems with a single user over AWGN channels. The timing error is uniformly distributed.

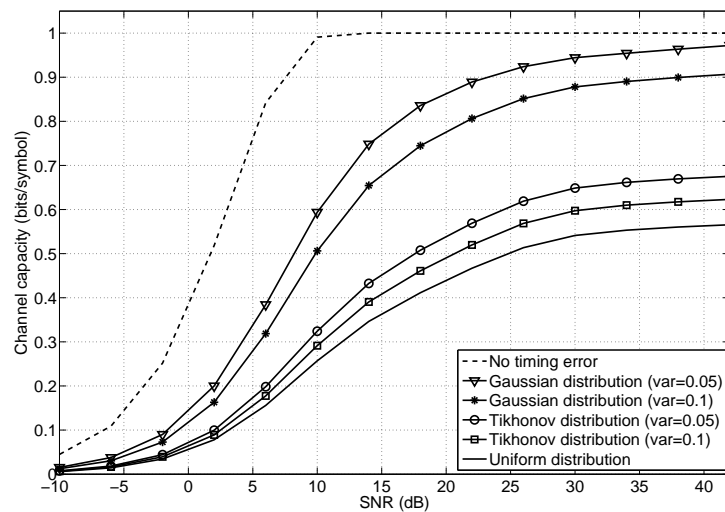


Fig. 2. Channel capacity v.s. SNR for the DS-BPSK system with/without timing error in an AWGN channel. The second-order derivative Gaussian pulse is used.

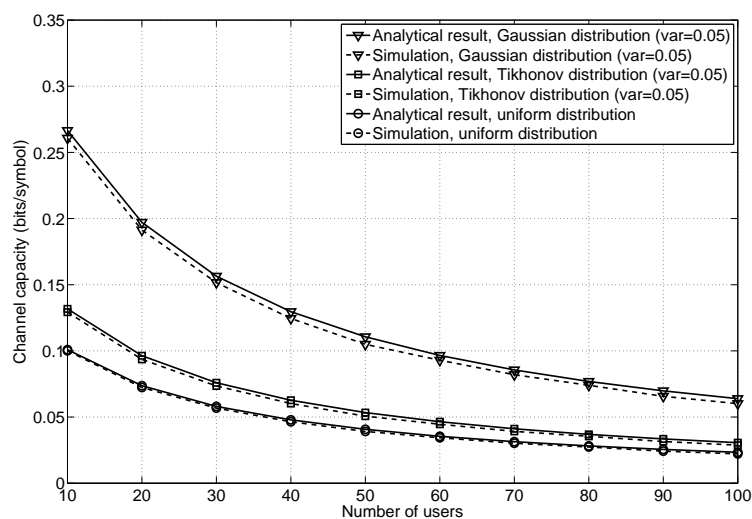


Fig. 3. Channel capacity per user v.s. the number of users for the DS-BPSK system with different timing error distributions in an AWGN channel. The second-order derivative Gaussian pulse is used.

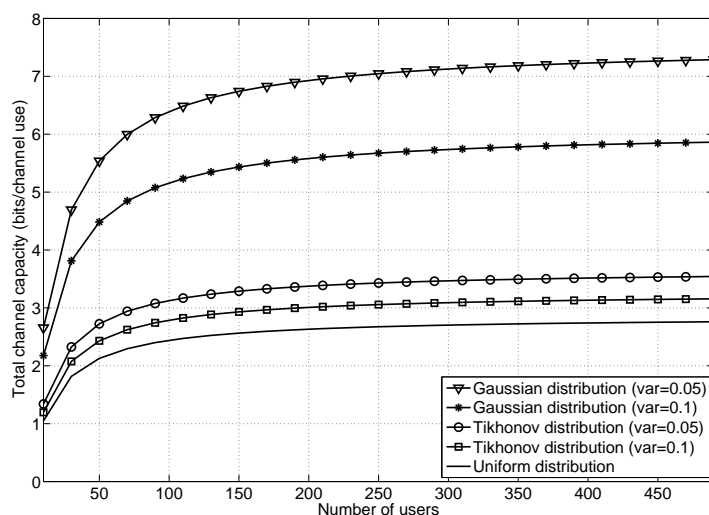


Fig. 4. Total channel capacity for all users v.s. the number of users for the DS-BPSK system with different timing error distributions in an AWGN channel. The second-order derivative Gaussian pulse is used.



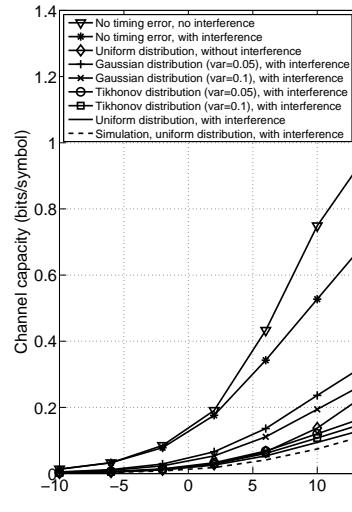


Fig. 5. Channel capacity v.s. SNR for the DS-BPSK system with/without the interferences and the timing error in the CM1 channel model. The second-order derivative Gaussian pulse is used.

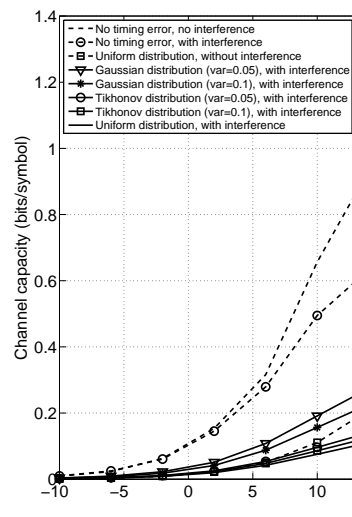


Fig. 6. Channel capacity v.s. SNR for the DS-BPSK system with/without the interferences and the timing error in the CM2 channel model. The second-order derivative Gaussian pulse is used.

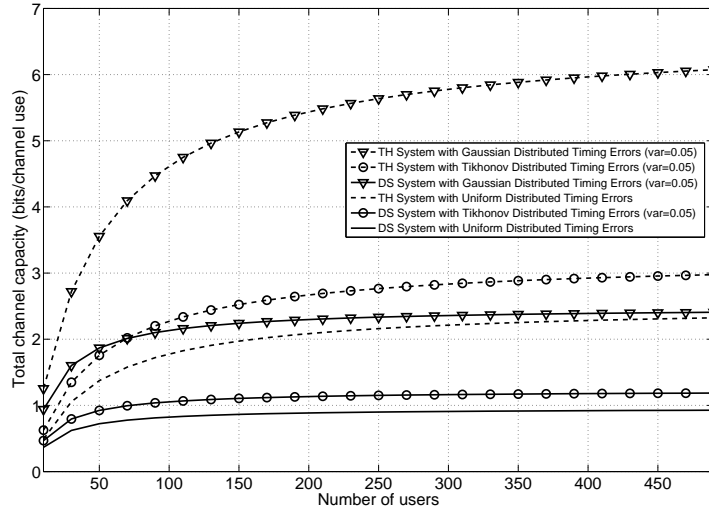


Fig. 7. Total channel capacity v.s. the number of users for the DS-BPSK and TH-BPSK systems with different timing error distributions in the CM1 channel model. The second-order derivative Gaussian pulse is used.

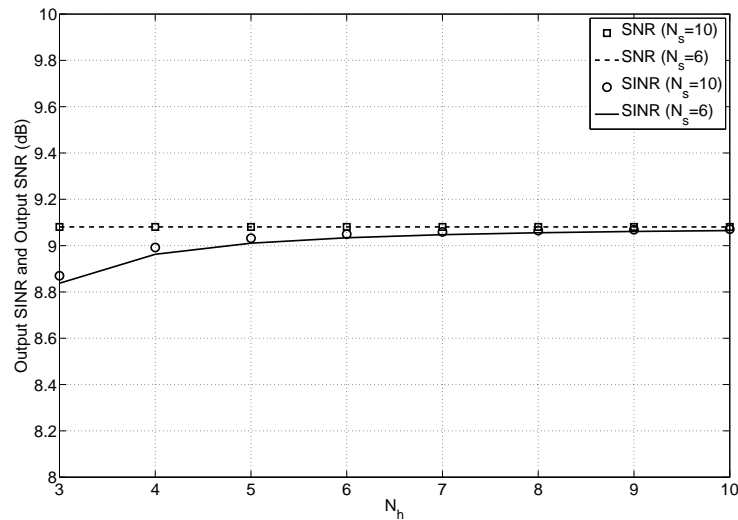


Fig. 8. Output SINR and output SNR v.s.  $N_h$  for the TH-BPSK system in an AWGN channel. The second-order derivative Gaussian pulse is used and the timing error is uniformly distributed.

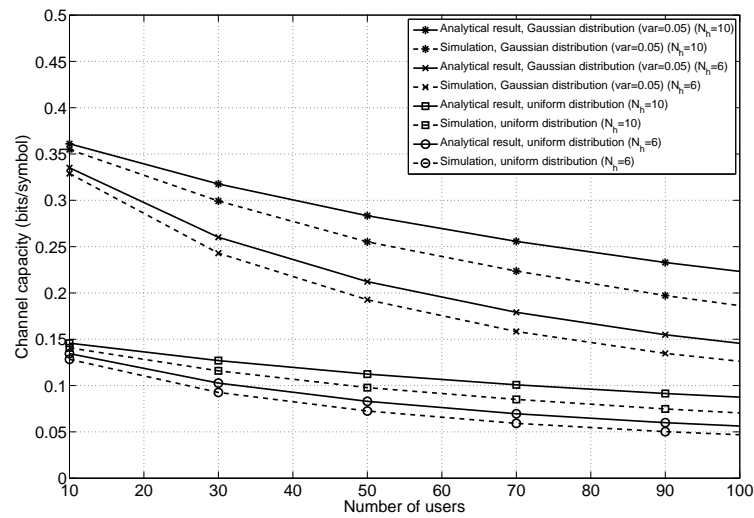


Fig. 9. Channel capacity per user v.s. the number of users for the TH-BPSK system with different timing error distributions in an AWGN channel. The second-order derivative Gaussian pulse is used.

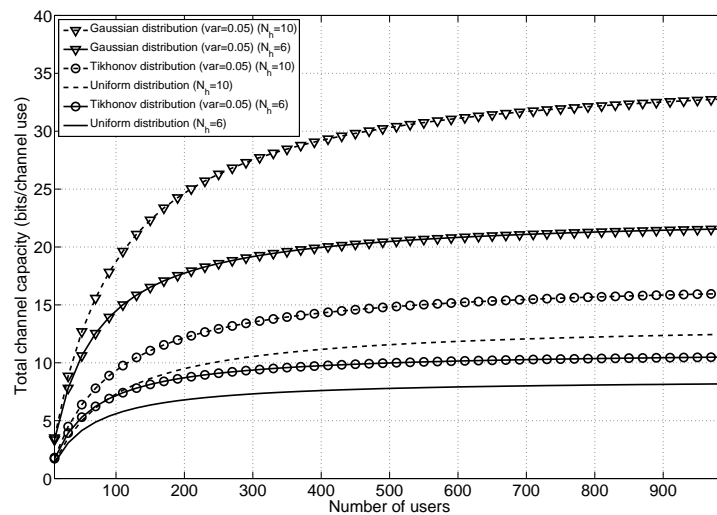


Fig. 10. Total channel capacity for all users v.s. the number of users for the TH-BPSK system with different timing error distributions in an AWGN channel. The second-order derivative Gaussian pulse is used.

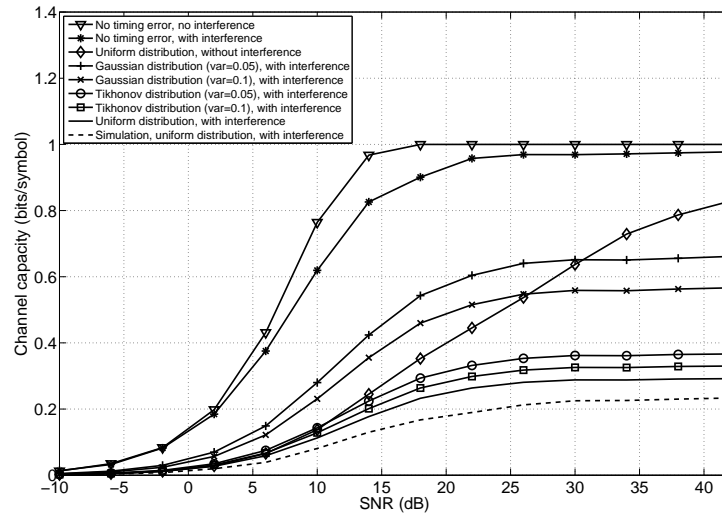


Fig. 11. Channel capacity v.s. SNR for the TH-BPSK system with/without the interferences and the timing error in the CM1 channel model. The second-order derivative Gaussian pulse is used.

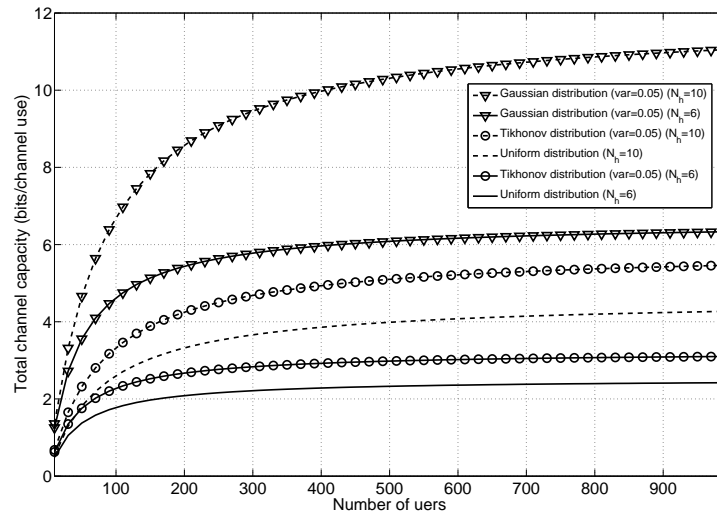


Fig. 12. Total channel capacity v.s. the number of users for the TH-BPSK system with different timing error distributions in the CM1 channel model. The second-order derivative Gaussian pulse is used.